DOI: https://doi.org/10.52756/ijerr.2023.v36.023 *Int. J. Exp. Res. Rev.*, Vol. 36: 232-243 (2023)

Original Article | *Peer Reviewed* | *Open Access*

International Journal of Experimental Research and Review (IJERR)

ISSN: 2455-4855 (Online)
www.iaph.in
ISSN 2455-4855

Experimental Study on Mechanical Behaviour of Arhar-Reinforced Composites using GRA with PCA

Venugopal Naidu Manubolu* and Diwakar Reddy Vanimireddy

Department of Mechanical Engineering, S.V.U. College of Engineering, Tirupati-517502, India

E-mail/Orcid Id:

VNM, venugopalnaidumanubolu@gmail.com, https://orcid.org/0000-0001-6752-3955;

DRV, vdrsvuce@gmail.com, https://orcid.org/0000-0003-1908-1368

Article History:

Received: 30th Sept., 2023
Accepted: 14th Dec., 2023
Published: 30th Dec., 2023

Keywords:

Arhar powder, FEA analysis, GRA and PCA, mechanical tests, SEM and XRD

How to cite this Article:

Venugopal Naidu Manubolu and Diwakar Reddy Vanimireddy (2023). Experimental Study on Mechanical Behaviour of Arhar-Reinforced Composites using GRA with PCA. *International Journal of Experimental Research and Review*, *36*, 232-243.

DOI:

https://doi.org/10.52756/ijerr.2023.v36.023

Abstract: The fiber composite plays a vital role in various applications in the current scenario. Natural fibers provide the desired advantages over synthetic fibers. Fiber composites deliver the exploration of durable, degradable, and lightweight materials. In several industrial sectors, transportation of materials from one place to another place is required. Materials like thermocoal boxes and iron boxes are inefficient in strength, weight, and cost. In order to overcome these, natural fiber-based composites, which give both strength and durability with low weight and cost, are chosen. This work explains the sample preparation using Arhar powder with an addition of reinforcements using the hand lay-up method by obeying the ASTM standards. To analyze the performance of the sample specimen, properties evaluated like Compression, Flexural, and other tests were conducted. GRA (Grey-Relational Analysis) with PCA (Principal-Component Analysis) was employed to carry out the most significant parameters, the most significant factor, and the weights of optimal parameters. Based on the output responses, it is experiential that the most effective parameter and best combination factor at Acrylonitrile butadiene styrene (ABS-4%), Guar Gum (8%), and Carboxy methyl cellulose (CMC-8%) with the values of 83.12 MPa compression strength, 61.70 MPa tensile strength and 0.249 joules of Impact strength.

Introduction

By the conservational effects (Om Prakash et al., 2018), industries are afraid of synthetic polymers (Kumar et al., 2014). Natural composites are made using organic fillers and are eco-friendly (Suzauddin et al., 2020), and they are termed Green composites (Jhamb et al., 2023). Natural composite materials are more adaptable because of their biodegradable nature and their availability. The desired properties of natural (Denise et al., 2012) composites are high strength, low cost, lightweight and inexhaustible (Sapuan et al., 2006; Joshi et al., 2004). It exhibits considerable mechanical behavior under loading variations. The researchers studied various bio-degradable polymer composites such as the orientation of fibers (Joshi et al., 2004), sawdust, banana woven (Nair et al., 2000), and sisal (Balakrishnan et al., 2022), and its reinforcement materials like shell-type and coconut fibers. The literature shows that natural materials (Sinha et al., 2020; Vijayan et al., 2022) come from plants with fibre components that enhance their strength. The material collected from the tree and added reinforcements in changing proportion levels and are tested in different aspects. In some parts of Andhra Pradesh state (Pramanik et al., 2021), after harvesting the Arhar crops (Riccardi et al., 2022), most of the farmers burned the remaining agricultural waste (Sarkar et al., 2019) such as plant branches, stem and roots (Sarkar et al., 2017) due to lack of rainfall (Sarkar and Maiti, 2020) to get decomposed naturally. Which emits carbon dioxide (Sarkar et al., 2020) and damages soil fertility (Sarkar et al., 2019). With this motivation, it is proposed to use plant-based agricultural waste like Arhar as the matrix material, which can greatly simplify the burning of agricultural waste.

Methodology

In this section, the process of specimen preparation, material selection, and design limitations are explained in the following.

***Corresponding Author:** venugopalnaidumanubolu@gmail.com

Workflow

The following process, as shown in Figure 1, is employed to study the mechanical characteristics and other aspects of immersion into commercial usage. A clear explanation of each section is given in the following.

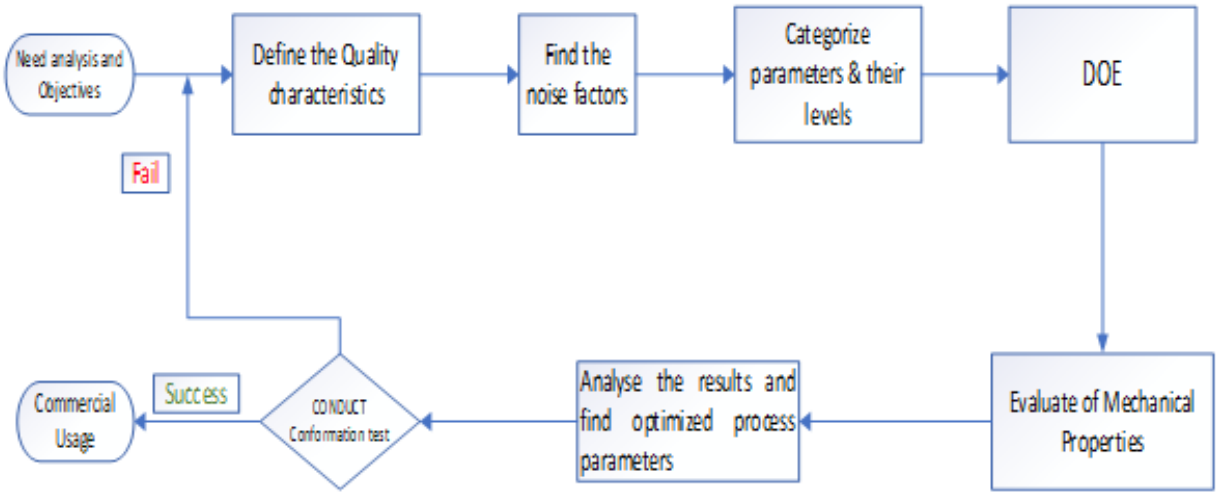

Figure 1. Workflow chart.

Analyzing the environmental effects, the following work objective is formulated to enhance the strength using natural degradation materials (Kerni et al., 2020). In this case, the Arhar material is chosen from agricultural waste (Saini et al., 2021), which consists of plant fibers and contributes to the strength of the material. Apart from this case, eco-friendly reinforcements like CMC, Guar Gum, and ABS are considered. Generally, the product characteristic depends on some parameters: reliability, functional ability, usability, availability, maintainability, and portability. In factor selection, each parameter consists of its levels, which are categorized depending on its properties when assorted with a matrix material. Here, 2%, 4%, and 6% were tested and it was noticed that there is vast scope to enhance its strength by changing/ increasing its composition levels. In this connection, the composition levels 4%, 8%, and 12% are chosen to study further behavior. The Hand lay-up method is used for preparing testing specimens and performing tests such as Flexural, Compression, Tensile, Impact tests, etc. to carry out Mechanical Characteristics. Hand Lay-up is a simple and effective process to fabricate natural composite materials using agricultural waste as matric material to prepare natural composite material. Further, the output responses were analyzed using Grey relational Grade (Pingulkar et al., 2021) and the Principal Component Analysis optimization technique to draw the most significant parameter. In transportation, using materials like thermocoal boxes and iron boxes is not efficient in strength, weight, and cost. In order to overcome these, natural fiber-based composites, which give both strength and durability with low weight and cost, are chosen.

Design of Experiments (DoE)

It is used to optimize the experiment conduction. In this work "3" factors with "3" levels are considered, as shown in Table 1(a). Minimum number of experiments to be carried out is 9 based on factors and levels, as shown in Table 1(b). Parameter-level design into an S/N ratio with the help of MINITAB V.14 (Om Prakash et al., 2018).

Table 1. DoE-based designed parameters

(a) Reinforcements with their levels.

Factors	Parameters	Levels
A	ABS	4% 8% 12%
B	Guar Gum	4% 8% 12%
C	CMC	4% 8% 12%

(b) Design of Experiments

Specimen No.	Process parameters (%)		
	ABS	Guar Gum	CMC
1	4	4	4
2	4	8	8
3	4	12	12
4	8	4	8
5	8	8	12
6	8	12	4
7	12	4	12
8	12	8	4
9	12	12	8

DOI: https://doi.org/10.52756/ijerr.2023.v36.023

Fabrication Process

The epoxy LY556 resin (Kamath and Chandrappa, 2022) with hardener 951 is considered in this work. It is blended completely in a beaker and then mixed 10:1 ratio thoroughly (Nayak et al., 2022) using a magnetic stirrer (de Kergariou et al., 2022) till a uniform mixture is obtained. The Arhar powder was treated as a matrix, and ABS, Guar gum and CMC were treated as reinforcements. Based on minerals such as cellulose etc., Arhar powder has properties similar to reinforcements. Foam mold (Yadav et al., 2020) was prepared to fabricate a specimen at room temperature at this time. Relative humidity is 53% using the hand lay-up method (Om Prakash et al., 2018) by following the procedure. A beaker filled with epoxy stirs up to a uniform mixture. Further, Arhar powder and reinforcements are added to the mixture and subsequently stirred. Furthermore, the mixture is poured on mold. To easily remove from mold and smooth surface finish Non-stick glass sheets are placed on the mold (Sk.Yusuf et al., 2020) and kept in an open environment to try the specimen. Further, it was removed from the workbench, and tests were performed to determine mechanical performance characteristics, as shown in Figure 2.

Performance of Mechanical Characteristics

The Specimens are prepared using Arhar powder and other reinforcements. The following tests are performed to study the mechanical behavior contrast and to draw the Mechanical Characteristics. The horizontal Tensiometer model PC-2000 is used to carry out the output responses from tensile-compression tests. It is also called mini UTM and has a capacity of 20KN. The testing specimen is placed on tensiometer grips with a 10 mm gauge length. The specimens for the compression test were prepared according to ASTM D3410 standards. The dimensions of the specimens are 140 mm in length, 20 mm wide, and 8 mm thickness. The specimens for the Tensile test were prepared according to ASTM D3039 standards. The dimensions of the specimens are 150 mm in length, 20 mm wide, and 8mm thick. The specimens for the Tensile test were prepared according to ASTM D256 standards. The dimensions of the specimens are 64 mm in length, 8 mm wide, and 8 mm in thickness. The specimens are shown in Figure 3 and Figure 4. Izod impact tests are performed on testing specimens to determine the impact strength of the surface with a default thickness of 8mm. A pivoting arm releases steady potential energy from a specific height and slams at a

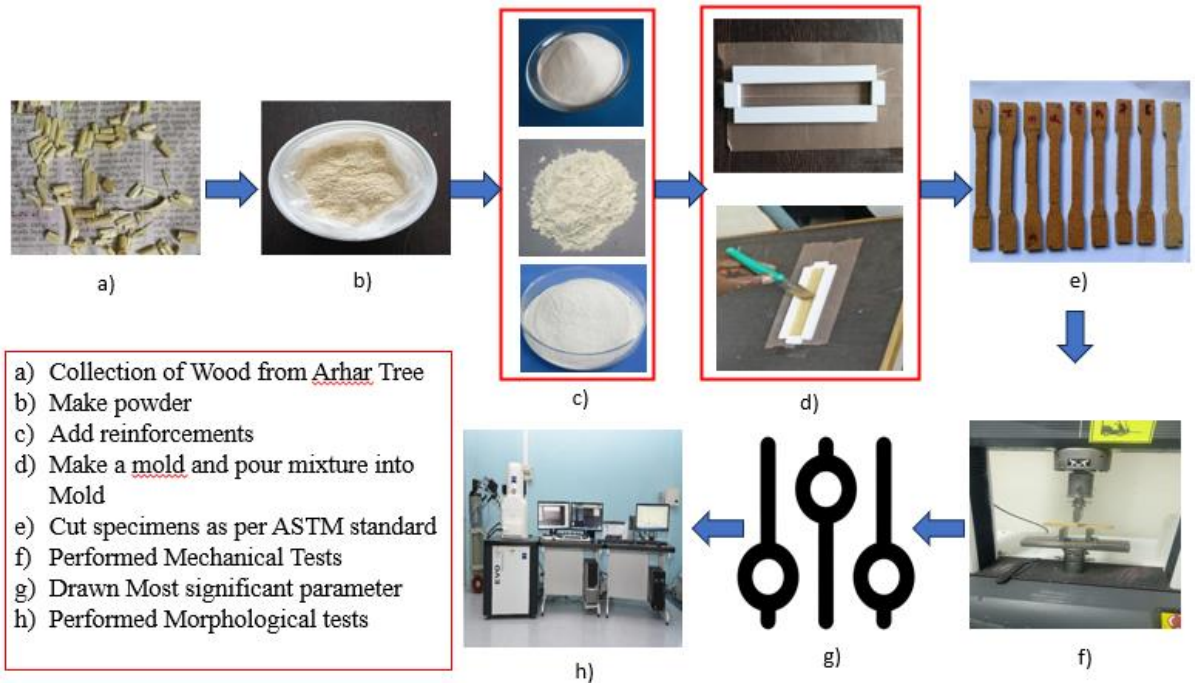

Figure 2. Specimen preparation process and testing.

DOI: https://doi.org/10.52756/ijerr.2023.v36.023

notched place on a sample. The capacity of the machine is 300J and the frequency capacity is up to 50 Hz.

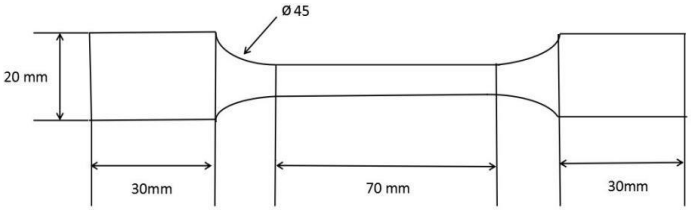

Figure 3. Specimen sizes according to ASTM standard

***Courtesy:** Tang **et al., 2022**

a) For Tensile test

b) For Compression test

c) For Izod Impact Test

Figure 4. Specimens based on ASTM standards.

As per the ASTM D2344-84, the testing specimens are prepared for the flexural test and the typical dimensions of the samples are 60 mm x 10 mm x 2 mm, and the loading rate (crosshead speed) is 2 mm/min. The flexural test (Tang et al., 2022) measures the material's strength and bending capability. There are two main types of tests to find flexural strength: the 4-point and 3-point bending tests. In the 3-Point bending test, the applied load at the center of the specimen is more accurate and gives better results, whereas, in the 4-Point bending test, the load is distributed to a large area. In 3-point bending, a digital encoder is used to measure the deflection, whereas a deflectometer is used in a 4-point bending test. The performance of a material can be effectively determined by using surface roughness tests (Joshi et al., 2004). It is defined based on the irregularities present on the material surface. There are different irregularities based on their size and shape. These irregularities may cause corrosion, nucleation sites, and cracks on the surface, resulting in the material's wear and tear. For better adhesion properties the roughness of a surface should be accurately determined. Getting a smooth surface requires a lot of machinery and several operations, making it the costliest, especially for composites.

SEM And XRD

Scanning Electron Microscopy (SEM) with Energy Dispersive Spectroscopy (EDS)

This is a mature technology used widely in scientific applications, especially materials metallurgy. The specimen surface is analyzed using scan coils, and that image reflects on a screen viewed by a microscope operator on a computer system. The scan coils detect the pure element on sample specimen for pure metals, but it will not do so for composites, for which sputter coating is applied (Nascimento et al., 2012) to Specimen to carry out the pure elements. So, it will act as a pure element. The usage of EDS in SEM analysis to completely understand involves the physical phenomenon, i.e., electron scattering component, X-ray fluorescence, and absorption scattering. The electron probe of 5mm is used to determine physical phenomena using X-rays. The SDD (Silicon drift detector) helps to absorb the X-ray reflection and Photoionization helps to detect the random direction.

X-ray diffraction (XRD)

It helps to carry out material structural properties using X-rays on microcrystalline samples. Bragg's law (Denise et al., 2012) helps to find d-spacing at a diffracting rate by using angle measurement where bright/thick spots appear. The scanning range employed in XRD is 3.000^{O}-90.000^{O} with a variance of 0.020^{0} and scan speed is 10.0000^{0} / minute. In this process, K-beta (X1) filter is used. K-β(X1) filter reduced the intensity of rays and Removed/Reduced background high-energy radiation compared to the K-α filter and other filters.

DOI: https://doi.org/10.52756/ijerr.2023.v36.023

Table 2. Output responses from various tests

Sl. No.	CS (MPa)	TS (MPa)	IS (Joules)	S/N1	S/N2	S/N3
1	82.63	62.08	0.227	38.343	35.859	12.879
2	83.12	61.70	0.249	38.394	35.806	12.076
3	82.75	63.43	0.293	38.355	36.046	10.663
4	82.41	61.49	0.195	38.320	35.776	14.199
5	82.40	62.67	0.227	38.319	35.941	12.879
6	82.32	62.52	0.249	38.310	35.920	12.076
7	82.54	62.79	0.216	38.333	35.958	13.311
8	82.82	62.09	0.227	38.363	35.860	12.879
9	82.95	62.26	0.26	38.376	35.884	11.701
			Min.	38.310	35.776	10.663
			Max.	38.394	36.046	14.199

GRA WITH PCA

Deng developed it, and the researchers identified its mechanical characteristics and substituted them with relative weights, which helps to draw significant parameters based on individual decision selection using GRA. Based on output response data carried out from basic analysis based on discrete principal components. It is uncorrelated to components as well as linear response variable combinations. The tool to optimize multi-performance characteristics is PCA. The note to be noted is that each response weight is not dependent nor equal to its relative revealing significance.

Results and Discussion

GRA with PCA

The following procedure is applied for the entire process to carry out significant parameters using GRA with PCA.

Step-1:- Find out SNRA (S/N ratios) value to output responses carried out by performing various tests shown in Table 2 using Eq. (1) (or) Eq. (2) (or) Eq. (3). In this process based on strength criteria Eq. (2) were employed.

High-quality parameter value small,

$$\eta = -10\log_{10}\left(\frac{1}{n}\right)\sum_{i=1}^{n}\frac{1}{y_{ij}^2} \quad \ldots\ldots\ldots\ldots\ldots\ldots \quad (1)$$

High-quality parameter value is large,

$$\eta = -10\log_{10}\left(\frac{1}{n}\sum_{i=1}^{n}y_{ij}^2\right) \quad \ldots\ldots\ldots\ldots\ldots\ldots \quad (2)$$

High-quality parameter value is neither large nor small,

$$\eta = 10\log_{10}\left(\frac{\mu^2}{\sigma^2}\right) \quad \ldots\ldots\ldots\ldots\ldots\ldots\ldots\ldots \quad (3)$$

Where, $\mu = \frac{y_1+y_2+y_3+\cdots\ldots+y_n}{n}$, $\sigma^2 = \frac{\sum(y_i-\bar{y})^2}{n-1}$, y_{ij} = Observed response value, n= No. of replications, j= 1,2,3……,k. and i= 1,2,3……,n

Table 3. Flexural test and Surface roughness analysis output responses

Sl. No	FS				RS(µm)	
	Maximum Load	Stress at Max. Load (MPa)	Strain at Max. Load	Flexural Modulus (GPa)	Min. Value	Max. Value
1	0.63	278.72	0.62	53.512	0.04	0.10
2	0.64	355.38	0.85	53.570	0.06	0.16
3	0.63	312.46	0.73	53.002	0.04	0.07
4	0.60	322.79	0.88	52.821	0.04	0.10
5	0.58	292.41	0.84	82.476	0.03	0.29
6	0.59	298.45	0.89	82.716	0.13	0.18
7	0.59	299.89	0.87	81.504	0.12	0.29
8	0.57	283.57	0.88	82.207	0.13	0.35
9	0.57	276.22	0.83	81.887	0.16	0.54

The single data input transformation in Normalization to split data evenly for further investigation in an acceptable range. The output response data is Compression Strength -CS, Tensile Strength-TS, Impact Strength-IS, Flexural Strength-FS, and Surface Roughness -SR, as shown in Table 2.

$$F = \frac{\mathrm{PL}}{(\mathrm{b}d^2)} \quad \ldots\ldots\ldots\ldots\ldots\ldots\ldots\ldots\ldots \quad (4)$$

Where "F" is "flexural strength", "d" is "beam deflection", "L" is "effective beam span", "P" represents "failure load", and "b" is "beam breadth". The output data responses are shown in Table 3 from FS and RS tests using Eq. (4).

Step-2: Normalization of y_{ij} as Z_{ij} ($0< Z_{ij} <1$) by adopting unit variation to minimize/ reduce variability.

DOI: https://doi.org/10.52756/ijerr.2023.v36.023

Normalizing the output data before analyzing it using GRA theory or other optimization techniques/methodologies is essential, as shown in Table 4.

Table 4. Normalization values for output responses.

Sl. No.	Normalization		
	CS	TS	IS
1	0.389	0.307	0.627
2	1.000	0.110	0.400
3	0.539	1.000	0.000
4	0.113	0.000	1.000
5	0.100	0.612	0.627
6	0.000	0.535	0.400
7	0.276	0.674	0.749
8	0.626	0.313	0.627
9	0.788	0.401	0.293

Step-3: By normalization, it predicts response sensitivity as shown in Table 5, and rank allocation based on our criteria. Eq. (5) (or) Eq. (6) (or) Eq. (7) normalize S/N ratio values by GRA. In this process based on strength criteria, Eq. (6) was employed.

High-quality parameter value small

$$Z_{ij} = \frac{Max(y_{ij}) - y_{ij}}{Max(y_{ij}) - Min(y_{ij})} \quad \ldots\ldots\ldots\ldots\ldots\ldots\ldots (5)$$

High-quality parameter value is large,

$$Z_{ij} = \frac{y_{ij} - Min(y_{ij})}{Max(y_{ij}) - Min(y_{ij})} \quad \ldots\ldots\ldots\ldots\ldots\ldots\ldots (6)$$

High-quality parameter value is neither large nor small,

$$Z_{ij} = \frac{(y_{ij} - Target) - Min(|y_{ij} - Target|)}{Max(|y_{ij} - Target|) - Min(|y_{ij} - Target|)} \quad \ldots\ldots\ldots\ldots (7)$$

Table 5. $\Delta_{oj}(k)$ from Normalization.

Sl. No	$\Delta_{oj}(k)$		
	CS	TS	IS
1	0.611	0.693	0.373
2	0.000	0.890	0.600
3	0.461	0.000	1.000
4	0.887	1.000	0.000
5	0.900	0.388	0.373
6	1.000	0.465	0.600
7	0.724	0.326	0.251
8	0.374	0.687	0.373
9	0.212	0.599	0.707
		Δ_{max}	1.000
		Δ_{min}	0.000

Step-4: Further, find out the GRC (Grey Relational coefficient) by applying Eq. (8) and Eq. (9) responses shown in Table 6.

$$\gamma(y_o(k), y_i(k)) = \frac{\Delta_{min} + \xi\Delta_{max}}{\Delta_{oj}(k) + \xi\Delta_{max}} \quad \ldots\ldots\ldots\ldots\ldots\ldots\ldots (8)$$

Ex. GRC for CS1 $= \frac{0+0.5((1)}{0.613+0.5(1)} = 0.449236 = 0.450$

Similarly, the remain GRC's calculated as in the following.

Where, k=1,2,3,……,m, m and n are No. of respondents and experiments data items, j=1,2,3,…….,n,

$y_i(k)$ = Specific sequence comparison, $y_o(k)$ = Sequence Reference.

Step-5: Absolute variation b/w $y_o(k)$ and $y_i(k)$ is,

$$\therefore \Delta_{oj} = \|y_o(k) - y_i(k)\| \quad \ldots\ldots\ldots\ldots\ldots\ldots\ldots (9)$$

$$\therefore \Delta_{min} = \min.min. \|y_o(k) - y_i(k)\| \quad \because$$

If value of $y_i(k)$ *is min.*

$$\therefore \Delta_{max} = \max.max. \|y_o(k) - y_i(k)\| \quad \because$$

If value of $y_i(k)$ *is max.*

$$\xi = Distingish\ co-efficient = 0 \leq \xi \leq 1$$

Table 6. GRC with grade system and Rank.

Sl. No	GRC			Grey Relation Grade	Rank
	CS	TS	IS		
1	0.450	0.419	0.573	0.481	8
2	1.000	0.360	0.454	0.605	2
3	0.520	1.000	0.333	0.618	1
4	0.360	0.333	1.000	0.565	3
5	0.357	0.563	0.573	0.498	7
6	0.333	0.518	0.454	0.435	9
7	0.408	0.605	0.666	0.560	4
8	0.572	0.421	0.573	0.522	6
9	0.703	0.455	0.414	0.524	5
Δ_{max}	1.000				
Δ_{min}	0.000				

By using GRA, effective parameters were identified. ABS was carried out at 12%, Guar Gum was at 12%, and CMC was at 8%.

Step-5: Computing co-relation co-efficient (R_{ij}) as shown in Eq. (10) using GRC responses shown in Table 7(a, b).

$$X_i = \begin{matrix} X_1(1) & X_1(2) & . & . & X_1(n) \\ X_2(1) & X_2(2) & . & . & X_1(n-1) \\ . & . & . & . & . \\ . & . & . & . & . \\ X_m(1) & X_m(2) & . & . & X_m(1) \end{matrix},$$

$$R_{ij} = \left[\frac{Cov(x_i(j)), x_i(l)}{\sigma_{x_i}(j) * \sigma_{x_i}(l)}\right] \quad \ldots\ldots\ldots\ldots\ldots\ldots\ldots (10)$$

DOI: https://doi.org/10.52756/ijerr.2023.v36.023

Table 7. Correlation and covariance coefficients.

(a) Covariance Matrix

CO-VARIANCE MATRIX		
0.041152	-0.00808	0.00861
-0.00808	0.036042	0.029246
0.00861	0.029246	0.034991

b) Co-rrelation coefficients

CO-RELATION MATRIX		
1	-0.20989	0.226887
-0.20989	1	0.823542
0.226887	0.823542	1

Where, j=1,2,3,…..,m, i=1,2,3…..,n and, $\sigma_{x_i}(j)$ & $\sigma_{x_i}(l)$ are variable responses of $j\&l$ standard deviation, $x_i(j)$ GRC response, $Cov(x_i(j))$ is a variable response of $j\&l$ covariance.

Subsequentially, carried eigen-values with their corresponding eigen-vectors using Eq. (11).

$$(R - \lambda_X I_m)V_{ik} = 0 \quad \text{.....(11)}$$

Where, "λ_X" "eigenvalues" and "V_{ik}" eigen-vectors corresponding to λ_X.

Table 8. Eigenvalues are based on the co-variance and correlation coefficients

Sl. No	EIGEN-VALUES	VARIATION
PC1	1.824	60.800
PC2	1.103	36.767
PC3	0.073	2.433

Further, carried out eigen-values & vectors shown in Table 8 then after finding PC (principal components) using Eq. (12).

$$Y_{mk} = \sum_{i=1}^{n} X_m(i)\, V_{ik} \quad \text{.....(12)}$$

Table 9. Eigen-vectors and Normalized eigenvectors with their principal weights.

Output Response	EIGENV-ECTORS			NORMALISED -VECTORS			PRINCIPAL WEIGHTS
	PC 1	PC2	PC3	PC 1	PC 2	PC 3	
CS	0.022	4.465	-0.47	0.016	0.949	-0.316	0.0002
TS	0.994	-1.105	-0.995	0.705	-0.235	-0.669	0.4968
IS	1	1	1	0.709	0.212	0.673	0.5028

Where, Y_{m1}, Y_{m2} are 1st and 2nd principal components and so on.

The action applied here concerning variance aligned principal components in descending order.

Step-6: Finally, GRG (Grey Relational Grade) was drawn from GRC using Eq. (13).

$$\gamma(X_o, X_i) = \frac{1}{m}\gamma\big(X_o(k), X_i(k)\big) \quad \text{(13)}$$

By analyzing principal weights as shown in Table 9. it is said that Tensile and impact strengths are influenced more by varying levels of composition.

SEM with EDS

The SEM results in the form of images are carried at 5µm,10µm, and 20µm magnifications. At 5µm shown in Figure 5(a, b)., it is seen that materials' shape. Few particles are bonded with each other as clusters. The gaps leave with other Particles cluster. Hence, it is also evident that particle sizes are approximately compatible and uniform based on XRD analysis.

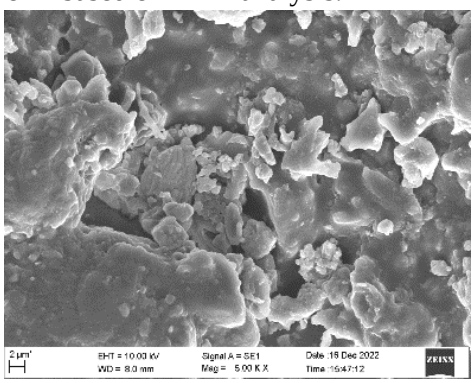

i)At 5µm

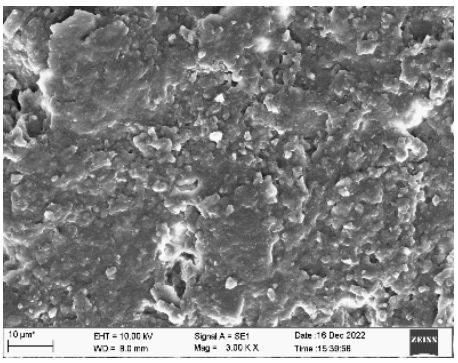

ii) At 10µm

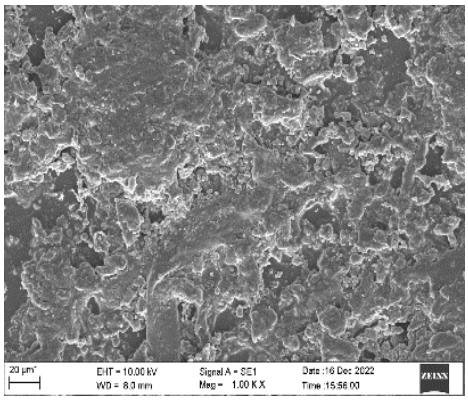

iii) At 20 µm

Figure 5 (a) Scanning Electron Microscopy (SEM) images before test

DOI: https://doi.org/10.52756/ijerr.2023.v36.023

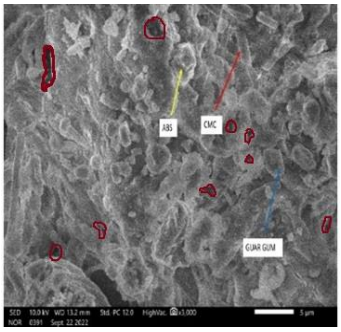

a) 5(µm)

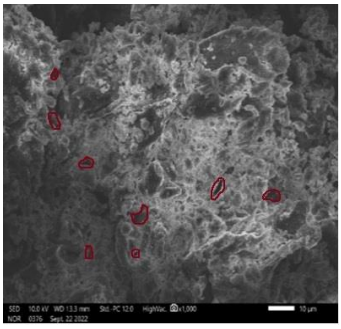

b) 10(µm)

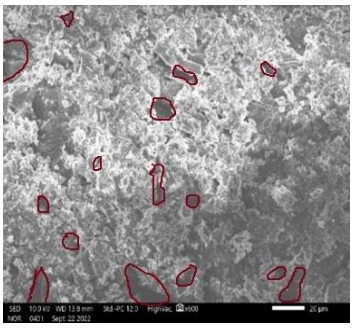

c) 20(µm)

Figure 5(b) SEM images after the test

It is observed that there are gaps and small size of cracks formed between the particulates after the test due to compaction while the load was applied to the specimen.

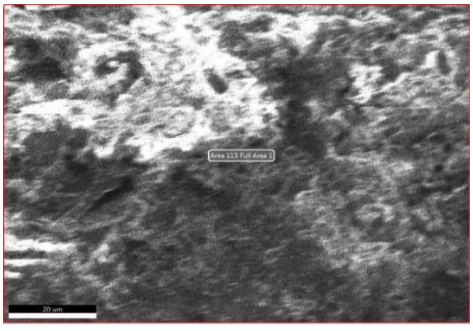

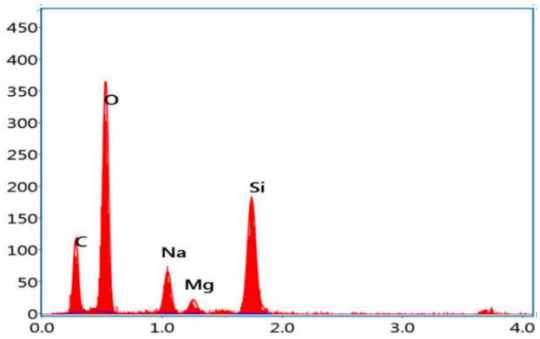

Figure 6. (a) EDS analysis area on sample; (b) Compound elements of sample in EDS.

By observing EDS analysis data as shown in Figure 6(a, b), the compound names identified are CMC, O, Guar gum, ABS, and Ca at different peak locations as shown in Table 10.

Table 10. The crystalline size of Arhar solid.

Sl. No	Element	Weight%	Atomic%
1	CMC K	55.01	67.28
2	O K	25.54	23.45
3	Guar gum K	6.12	3.33
4	ABS K	7.52	3.33
5	Ca K	5.80	2.61

X-Ray Diffraction

XRD test was performed on testing specimens, and results are shown in Figure 7. Area reduction under peaks results in a crystalline region with an amorphous nature. Before calcination, the XRD peaks at vigorous intensity reveal that have better crystallinity for precursor particles. Minor peaks disappearance /contamination peaks angles" in particle XRD shows calcination crystallinity-reaction. The average particle/grain size was measured by applying Scherrer's equation in Eq. (14).

$$D=\frac{K*\lambda}{\beta*cos\theta} \quad \text{.....(14)}$$

Where,

"λ" is X-ray wavelength, 0.15406 "JCPDS25-1079", "D" is "Crystal Mean size" in "mm", "K" is "Crystalline shape factor constant" equal to 0.89, "Θ" is "Bragg's angle" at absolute peak, "β" represents "full-width half maximum (FWHM)".

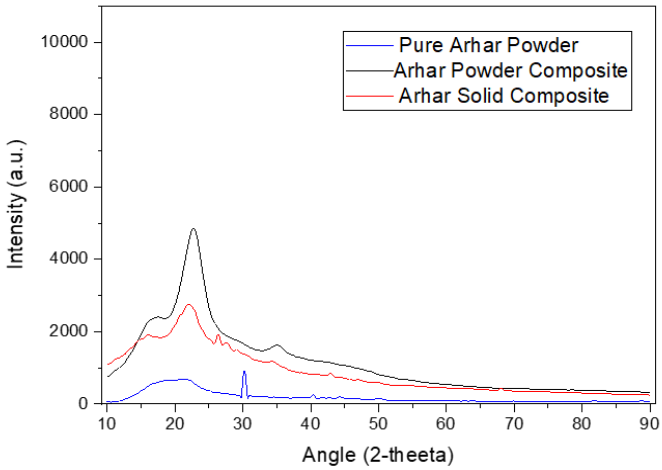

Figure 7. XRD for Arhar composite (2 Theta Vs. Intensity)

The degree of crystallinity/ structure of a material is defined using this test. The peaks are identified as shown in Table 11.

Table 11. The crystalline size of Arhar solid.

2θ (degrees)	d-spacing	θ(degrees)	θ(radians)	FWHM (deg.)	FWHM(β) (rad.)	D (nm)
30.247	3.035	15.123	0.263	0.157	2.740*10-3	52.853
40.379	2.285	20.189	0.352	0.059	1.029*10-3	140.737
44.103	2.095	22.051	0.384	0.157	2.740*10-3	52.853
Crystalline size(nm)						246.443
Average crystalline size (nm)						82.147

Fourier Transformation Infrared (FTIR) Test

The solid infrared spectrum emission/ absorption, or gas, is obtained using FTIR techniques. An FTIR-spectrometer simultaneously collects top spectral data resolution over a hefty spectral range. This gives a major advantage over a dispersive spectrometer, it measures intensity over a small range at a single wavelength. The phrase "Fourier Transfer Infrared Spectroscopy" comes from the fact that raw data could transformed into a spectrum by Fourier transform. The testing was carried out using the experimental machine CARY 630 FTIR (Rajini et al., 2021). Need the transmittance value to figure out the wave number (Venkata and Damodar, 2023). For all of the samples, using a range of 4000~400cm-1. The FTIR results are carried out at the range 4000~500 cm-1 as shown in Figure 8, the FTIR testing of the sample has found 12 peaks of functional group Wavenumber.

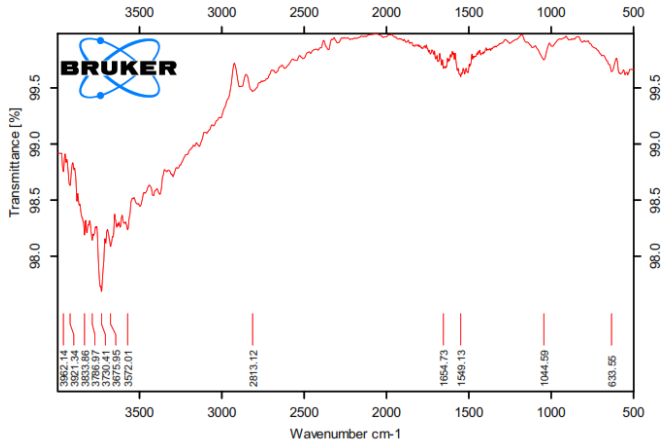

Figure 8. FTIR result for Sample ABS(4%), Guar gum(8%) and CMC (8%).

The peaks of fundamental group Wave numbers are 633.55, 1044.59, 1549.13, 1654.73, 2813.12, 3572.01, 3675.95, 3730.41, 3786.97, 3833.86, 3921.34, 3962.14. According to standard FTIR reference data, it is observed that the absorption bond at 633.55 wavenumbers found symmetrical stretching vibration of the tetrahedron, and the strong broad found at 1044.59 was related to CO-O-CO stretching under excitation of anhydride. The strong broad found at 1549.13 was related to N-O stretching nitro compound. The strong broad found at 1654.73 was related to C=O stretching δ-lactam compound. The medium broad found at 2813.12 was related to doublet C-H stretching aldehyde compound. The medium sharp O-H stretching found at 3730.41 was related to the free alcohol compound.

Comparative Study

Based on previous researchers' work, the specimens are selected as new base materials and prepared and tested to draw various characteristics. Further, the output responses are compared with previous researchers' work whether improved or not and are represented in Figure 9.

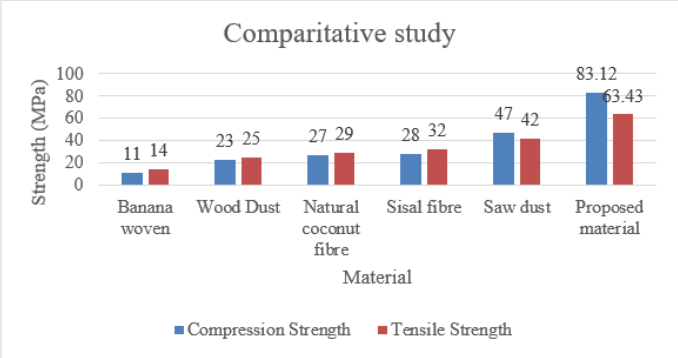

Figure 9. Comparative analysis between past and proposed work.

Figure 8 represents the Comparative analysis between the past and this work, it is noticed that material strength has been considerably improved. From the SEM analysis, it is observed that gaps and small cracks formed between the particulates after the test.

Finite Elemental Analysis (FEA) for Transport Application

Based on the output responses received from the various tests, as shown in Tables 2 & 3, it is observed that there is scope to use in the transport application instead of Thermocol and other expensive packaging units. In this connection, the FEA analysis performed on the sample design is shown in Figure 10(a). Bike transport in railway transportation is considered for an application. Generally, the average bike dimension is 254mm in length, 100 mm in width, and 150mm in height. Based on the following dimensions, the transport box was designed and performed FEA on design components and following results were carried out. Generally, the bike's weight is 300 lbs. Newtons is a 1500N load applied on the bottom and top of the box surface, as shown in Figure 10(b).

DOI: https://doi.org/10.52756/ijerr.2023.v36.023

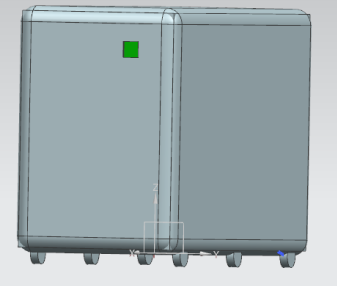

i) Sample Design

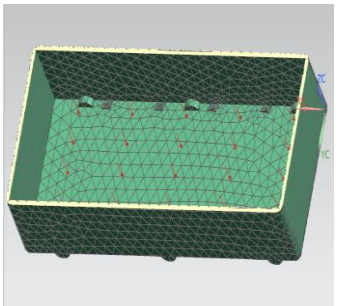

ii) Load applied on the box

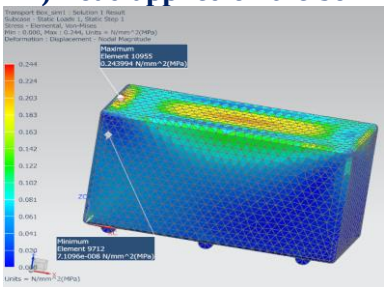

iii) FEA of the box

Figure 10. Finite analysis images on transportation box.

The following results are drawn from the finite element analysis, as shown in Table 12.

Table 12. Finite element analysis for Transportation box.

Load type	Elemental stress (MPa)	Nodal displacement (mm)	Nodal stress (MPa)
Bending	0.0512	0.24399	0.5027
Compression	0.051	0.2266	0.5144
Tensile	0.0412	0.1836	0.4184

From the results of finite element analysis, the transport box has the bike load capability and it can be stated that it may be suitable for the transport application in railway transportation.

Conclusion

The behavioral performance of Arhar composites has been studied in composition variations as a function of compression strength, tensile strength, etc. It is noticed that the most significant parameter and best combination factor at Acrylonitrile butadiene styrene (ABS-4%), Guar Gum (8%), and Carboxy methyl cellulose (CMC-8%) with the values of 83.12 MPa compression strength, 61.70 MPa tensile strength and 0.249 joules of Impact strength. From the SEM images at the point of load concentration, it can be observed that the particulates are deformed due to the small size of cracks and gaps formed. Compression strength is a more significant principal component when compared with tensile and impact strength. The output responses stated the efficacious fabrication of Arhar composites. It is confirmed that Arhar Powder is used as filler material to enhance the strength. Based on output responses, Arhar composite material may be possible to use in industrial applications where strength is the main criteria. This material may be used in place of transportation in its place of Thermocol and other exclusive packaging units.

Acknowledgement

The authors declare that they have no known competing financial interests or personal relationships that could have appeared to influence the work reported in this paper.

Conflicts of Interest

The authors declare no conflict of interest.

References

Balakrishnan, M.E.N., Muralkar, P.K., Ponraj, M.R., Nadiger, S., Dhandayutham, S., Justus, S., & Bhagavathsingh, J. (2022). Recycling of sawdust as a filler reinforced cotton seed oil resin amalgamated polystyrene composite material for sustainable waste management applications. *Materials Today: Proceedings*, *58*(2),783-78. https://doi.org/10.1016/j.matpr.2022.03.331

de Kergariou, C., Chul Kim, B.C., Perriman, A., Duigou, A.L., Guessasma, S., & Scarpa, F. (2022). Design of 3D and 4D printed continuous fiber composites via an evolutionary algorithm and voxel-based Finite Elements: Application to natural fiber hygromorphs. *Additive Manufacturing*, 59(A), 1-12. https://doi.org/10.1016/j.addma.2022.103144

Jhamb, S. K., Goyal, A., Pandey, A., & Verma, M. N. (2023). Mechanical, Wear, and Degradation Behavior of Biodegradable Mg-x% Sn Alloy Fabricated through Powder Mixing Techniques. *Journal of Materials Engineering and Performance*, *32*, 7123–7133. https://doi.org/10.1007/s11665-022-07620-8

Joshi, S.V., Drzal, L.T., Mohanty, A.K., & Arora, S. (2004). Are natural fiber composites

environmentally superior to glass fiber reinforced composites? *Composites Part A: Applied Science and Manufacturing*, *35*(3), 371-376. https://doi.org/10.1016/j.compositesa.2003.09.016

Kamath, S.S., & Chandrappa, R.K. (2022). Additives used in natural fiber reinforced polymer composites-a review, *Materials Today: Proceedings*, *50*(5), 1417-1424. https://doi.org/10.1016/j.matpr.2021.08.331

Kerni, L., Singh, S., Patnaik, P., & Kumar, N. (2020). A review on natural fiber reinforced composites. *Materials Today: Proceedings*, *28*(3), 1616-1621. https://doi.org/10.1016/j.matpr.2020.04.851

Kumar, R., Kumar, K., & Bhowmik, S. (2014). Optimization of mechanical properties of epoxy-based wood dust reinforced green composite using Taguchi method. *Procedia Materials Science*, *5*, 688-696. https://doi.org/10.1016/j.mspro.2014.07.316

Nair, K.C.M., Kumar, R.P., Thomas, S., Schit, S.C., & Ramamurthy, K. (2000). Rheological behavior of short sisal fiber- reinforced polystyrene composites. *Composites Part A: Applied Science and Manufacturing*, *31*(11), 1231-1240. https://doi.org/10.1016/S1359-835X(00)00083-X

Nascimento, D.C.O., Ferreira, A.S., Monteiro, S.N., Aquino, R.C.M.P., & Kestur, S.G. (2012). Studies on the characterization of piassava fiber and their epoxy composites. *Composites Part A: Applied Science and Manufacturing*, *43*(3), 353-362. https://doi.org/10.1016/j.compositesa.2011.12.004

Nayak, S., Jesthi, D.K., Saroj, S., & Sadarang, J. (2022). Assessment of impact and hardness property of natural fiber and glass fiber hybrid polymer composite. *Materials Today: Proceedings*, 49(2), 497-501. https://doi.org/10.1016/j.matpr.2021.03.079

Om Prakash, M., Raghavendra, G., Panchal, M., S. Ojha, S., & Bose, P.S.C. (2018). Influence of distinct environment on the mechanical characteristics of Arhar fiber polymer composites. *Silicon*, *10*, 825-830. https://doi.org/10.1007/s12633-016-9536-3

Pingulkar, H., Mache, A., Munde, Y., & Siva, I. (2021). A comprehensive review on drop weight impact characteristics of bast natural fiber reinforced polymer composites. *Materials Today: Proceedings*, *44*(5), 3872-3880. https://doi.org/10.1016/j.matpr.2020.12.925

Pramanik, A., Sarkar, S., Maiti, J., & Mitra, P. (2021). RT-GSOM: Rough tolerance growing self-organizing map. *Information Sciences*, *566*, 19-37. https://doi.org/10.1016/j.ins.2021.01.039

Rajini, B., Narasimha, R.A.V., & Sashidhar, C. (2021). Micro-level studies of fly ash and GGBS –based geopolymer concrete using Fourier transform Infra-Red. *Materials Today: Proceedings*, *46*(1), 586-589. https://doi.org/10.1016/j.matpr.2020.11.291

Riccardi, M.R., Mauriello, F., Sarkar, S., Galante, F., Scarano, A., & Montella, A. (2022). Parametric and Non-Parametric Analyses for Pedestrian Crash Severity Prediction in Great Britain. *Sustainability*, *14*(6), 3188. https://doi.org/10.3390/su14063188

Saini, M.K., Bagha, A.K., Kumar, S., & Bahl, S. (2021). Finite element analysis for predicting the vibration characteristics of natural fiber reinforced epoxy composites. *Materials Today: Proceedings*, *41*(2), 223-227. https://doi.org/10.1016/j.matpr.2020.08.717

Sapuan, S. M., Leenie, A., Harimi, M., & Beng, Y.K. (2006), Mechanical Properties of Woven banana fiber Reinforced Epoxy Composites. *Materials and Design*, *27*(8), 689-693. https://doi.org/10.1016/j.matdes.2004.12.016

Sarkar, S., & Maiti, J. (2020). Machine learning in occupational accident analysis: A review using science mapping approach with citation network analysis. *Safety Science*, *131*, 104900, https://doi.org/10.1016/j.ssci.2020.104900

Sarkar, S., Baidya, S., & Maiti, J. (2017). Application of rough set theory in accident analysis at work: A case study, *Third International Conference on Research in Computational Intelligence and Communication Networks (ICRCICN)*, pp. 245-250. http://dx.doi.org/10.1109/ICRCICN.2017.8234514

Sarkar, S., Chain, M., Nayak, S., & Maiti, J. (2019). Decision Support System for Prediction of Occupational Accident: A Case Study from a Steel Plant. *Emerging Technologies in Data Mining and Information Security, Part of Advances in Intelligent Systems and Computing*, *813*,7 87-796, Springer, Singapore. https://doi.org/10.1007/978-981-13-1498-8_69

Sarkar, S., Pramanik, A.P., Maiti, J., & Genserik, R. (2020). Predicting and analyzing injury severity: A machine learning-based approach using class-imbalanced proactive and reactive data. *Safety Science*, *125*, 104616. https://doi.org/10.1016/j.ssci.2020.104616

Sarkar, S., Vinay, S., Raj, R., Maiti, J., & Mitra, P. (2019). Application of optimized machine learning techniques for prediction of occupational accidents. *Computers & Operations Research*, *106*, 210-224. https://doi.org/10.1016/j.cor.2018.02.021

Sinha, R.K., Sridhar, K., Purohit, R., & Malviya, R.K. (2020). Effect of nano SiO_2 on properties of natural fiber reinforced epoxy hybrid composite: A review. *Materials Today: Proceedings*, *26*(2), 3183-3186. https://doi.org/10.1016/j.matpr.2020.02.657

Sk.Yusuf, S., Md. Islam, N., Md. Akram, W., Md. Ali, H., & Md. Siddique, A. (2020). Prediction of the best tensile and flexural strength of natural fiber reinforced epoxy resin-based composite using Taguchi method. *Proceedings of the International Conference on Industrial & Mechanical Engineering and Operations Management*. http://www.ieomsociety.org/imeom/168.pdf

Tang, L., Liu, T., Sun, P., Wang, Y., & Liu, G. (2022). Sisal fiber modified construction waste recycled brick as building material: Properties, performance and applications. *Structures*, *46*, 927-935. https://doi.org/10.1016/j.istruc.2022.10.126

Venkata, A.K.G., & Damodar, R. M. (2023). TLBO-trained ANN-based Shunt Active Power Filter for Mitigation of Current Harmonics. *International Journal of Experimental Research and Review*, *34*(Special Vol), 11-21. https://doi.org/10.52756/ijerr.2023.v34spl.002

Vijayan, R., Bharani, C.J., Rathinasuriyan, C., Palanisamy, R., & Thanka, G. T. (2022). Viscoelastic behavior of natural fiber reinforced composite material. *Materials Today: Proceedings*, *52*(3), 1942-1945. https://doi.org/10.1016/j.matpr.2021.11.592

Yadav, R., Gupta, R. K., & Goyal, A. (2020). Study of tribological behavior of hybrid metal matrix composites prepared by stir casting method. *Materials Today: Proceedings*, *28*(4), 2218-2222. https://doi.org/10.1016/j.matpr.2020.04.527.

How to cite this Article:
Venugopal Naidu Manubolu and Diwakar Reddy Vanimireddy (2023). Experimental Study on Mechanical Behaviour of Arhar-Reinforced Composites using GRA with PCA. *International Journal of Experimental Research and Review*, *36*, 232-243.

DOI : https://doi.org/10.52756/ijerr.2023.v36.023